AGU PUBLICATIONS

Geophysical Research Letters

RESEARCH LETTER
10.1002/2014GL060062

Key Point:
- Airborne radar reveals sea spray mass profiles at tropical storm wind speeds

Correspondence to:
C. W. Fairall,
Chris.fairall@noaa.gov

Citation:
Fairall, C. W., S. Pezoa, K. Moran, and D. Wolfe (2014), An observation of sea-spray microphysics by airborne Doppler radar, *Geophys. Res. Lett.*, *41*, doi:10.1002/2014GL060062.

Received 27 MAR 2014
Accepted 8 MAY 2014
Accepted article online 14 MAY 2014

An observation of sea-spray microphysics by airborne Doppler radar

C. W. Fairall[1], S. Pezoa[1], K. Moran[2], and D. Wolfe[2]

[1]NOAA, Earth System Research Laboratory, Boulder, Colorado, USA, [2]Cooperative Institute for Research in Environmental Science, University of Colorado, Boulder, Colorado, USA

Abstract This paper describes observations and analysis of Doppler radar data from a down-looking 94 GHz (W-Band) system operated from a NOAA WP-3 Orion research aircraft in Tropical Storm (TS) Karen. The flight took place on 5 October 2013; Karen had weakened with maximum winds around 20 m s^{-1}. Doppler spectral moments from the radar were processed to retrieve sea-spray microphysical properties (drop size and liquid water mass concentration) profiles in the height range 75–300 m above the sea surface. In the high wind speed regions of TS Karen ($U_{10} > 15$ m s^{-1}), sea spray was observed with a nominal mass-mode radius of about 40 μm, a radar-weighted gravitational fall velocity of about 1 m s^{-1}, and a mass concentration of about 10^{-3} gm^{-3} at 75 m. Spray-drop mass concentration declined with height to values of about 10^{-4} gm^{-3} at 300 m. Drop mass decreased slightly more slowly with increasing height than predicted by surface-layer similarity theory for a balance of turbulent diffusion vs fall velocity.

1. Introduction

Present parameterizations of air-sea turbulent fluxes are reasonably valid up to wind speeds of about 25 m s^{-1} [*Fairall et al.*, 2003; *Drennan et al.*, 2007; *Edson et al.,* 2013]. This wind speed range covers the vast majority of oceanic wind climatology. Extrapolations of the current parameterizations to hurricane wind speeds are inconsistent with theoretical analyses of the potential strength of tropical cyclones [*Emanuel*, 1995]. One major issue is the relative balance of momentum and scalar (heat/moisture) transfers—usually expressed as the ratio of the enthalpy transfer to the momentum transfer coefficients. It is speculated that the heat and moisture balance is affected by evaporation of sea-spray droplets at very high wind speeds ($U_{10} > 25$ m s^{-1}). At high wind speeds, the ocean is a major source of droplets produced by bursting bubbles and spume (i.e., from sheared-off wave tops) to the lower troposphere [*Andreas et al.*, 1995]. Because of their much larger sizes (and larger mass flux), spume droplets are expected to dominate the droplet aspects of the hurricane flux problem.

Droplets may play a significant role in latent heat transfer between the ocean and atmosphere [*Andreas et al.*, 1995] and, under extremely high winds such as found in hurricanes, may also have a large effect on the air-sea exchange of momentum [*Andreas and Emanuel,* 2001; *Andreas,* 2004; *Kudryavtsev and Makin*, 2011]. Recent numerical modeling studies have shown hurricane intensity to be quite sensitive to representation of surface fluxes and sea spray [e.g., *Bao et al.,* 2011]. From a modeling perspective, there are two fundamental problems: (1) specification of the sea surface droplet source strength and (2) computation (or parameterization) of the thermodynamic effects of the sea spray [*Fairall et al.,* 1990, 1994; *Kepert et al.*, 1999; *Bianco et al.*, 2011; *Richter and Sullivan*, 2014].

The fundamental parameter used for representing the effect of sea spray on air-sea exchange processes is the size dependent source function, $S_n(r)$, or the number of droplets of a given size produced at the sea surface per unit surface area per unit time, as a function of the surface forcing (wind speed, wave breaking, surface stress, etc.)—see *Fairall et al.* [2009] for a summary. Because the source function cannot be measured directly at present, it is typically estimated from the height (z)-dependent size concentration (radius, r) distribution of droplets, $n(r,z)$. The relationship between the source strength, the atmospheric turbulence profiles, the forcing, and the profiles of droplet concentration as a function of droplet size is key to this approach.

Extreme storm conditions over the ocean are experimentally challenging to near-surface observations of aerosols and turbulence. Ships prefer to avoid such conditions, research aircraft prefer to avoid low-level operations in hurricanes, and fixed platforms offer rare sampling opportunities and likely disturb the

observations. In 2003, the Earth System Research Laboratory (ESRL) made droplet measurements with an optical spectrometer from a NOAA WP-3 from level runs at altitudes from 66 to 750 m in hurricanes Fabian and Isabel as part of the Coupled Boundary Layer/Air-Sea Transfer (CBLAST) project [*Black et al.*, 2007]. Wind speeds were on the order of 23 m s^{-1} and, at the nominal aircraft altitude (~100 m), droplet concentrations were close to the sensitivity threshold of the instrument. Furthermore, it was quite difficult to ensure the observations were not contaminated by precipitation. Ironically, after problems with aircraft engines ingesting *sea salt* during the low-level runs in CBLAST, NOAA has put a hold on low-level flights in hurricanes. Thus, high-quality in situ measurements of sea-spray drop size spectra at winds exceeding 25 m s^{-1} are essentially non-existent [see the recent review by *Jones and Andreas,* 2012], and, barring a breakthrough in remotely-piloted or disposable vehicles, prospects for future data at wind speeds of 50 m s^{-1} are quite poor.

Following the CBLAST experience, we began to explore airborne remote sensing approaches to observing sea spray in high winds. Lidar have some potential [*Toffoli et al.,* 2011], but rely on a clear-air line of sight to the surface and may be too sensitive to more abundant small aerosols. Airborne millimeter-wavelength radar offers an attractive option for such measurements [*Esteban-Fernandez et al.*, 2010; *Yurovsky and Malinovsky,* 2012]. Compared to conventional centimeter-wavelength radars, they offer advantages in greater sensitivity to sea-spray droplet sizes, finer vertical resolution, and faster sample rates. In this paper, we will present results from a single flight with the ESRL 94-GHz (3.17 mm wavelength) W-Band Doppler radar [*Moran et al.*, 2012] in Tropical Storm (TS) Karen in October 2013. The analysis is complex, but we offer clear evidence that sea spray is observed by the radar in the altitude range 75–300 m above the surface. The 25 m range resolution and contamination of the signal by the strong surface return restrict our retrieval to a minimum altitude of 75 m. Deduced liquid water concentrations are small but comparable to the limited estimates available in the literature.

2. Observational Details

This study was done in TS Karen (see http://www.nhc.noaa.gov/data/tcr/AL122013_Karen.pdf for details). The observations were taken with the aircraft at an altitude of 2300 m during a 6 h flight on 5 October 2013. Flight track and altitude in the period of data sampling are shown in Figure 1. The aircraft operated from the Tampa, FL area; TS Karen was centered at 27.5 N lat. and 91.5 W lon. The high wind region for Karen was in the NE quadrant of the storm; maximum 10 m wind was 20 m s^{-1} with 25% of the U_{10} values in the experimental area exceeding 15 m s^{-1}. A second NOAA WP-3 made flights on 3 and 4 October measured surface wave properties using a scanning radar altimeter [*Walsh et al.,* 1985]. On 4 October, maximum significant wave heights were about 4.5 m (see http://prosensing.com/wsradisplay/index.php?hurricaneID=20131004H_Karen).

The WP-3 observing systems used for this study include the ESRL W-Band radar, the Stepped Frequency Microwave Radiometer (SFMR), dropsondes, and the aircraft flight-level meteorology and navigational data. The W-Band radar is described extensively by *Moran et al.* [2012], so we offer only a brief summary here. It was repackaged from its original ship-based form to fit in a small windowed compartment on the WP-3, but the basic operation is similar to the ship (except it is down-pointing on the aircraft). The W-Band is a coherent, pulsed Doppler radar with a beam width of 0.7° operating at 94 GHz; a 128 point Doppler spectrum is produced every 0.3 s at 150 range gates with 25 m range resolution; the first range gate is 500 m below the aircraft, and the last is 4250 m below. For each spectrum, standard spectral processing is used [*Moran et al.,* 2012]. The peak of the return is identified, and the spectral noise level is computed. The first three moments of the Doppler spectra are computed and archived with the raw spectra. These moments correspond to the 0.3 s and 25 m returned radio-frequency power (zeroth moment spectral density above the noise level), mean Doppler shift (first moment), and the Doppler width of the return (second moment about the mean).

An example of the three moments is shown (Figure 2) as a time-height cross section for 1 h beginning at 0700 UT—height is positive upward referenced to the surface. The radar is fixed to the airframe, so aircraft motion and orientation from the WP-3 flight level and navigational measurements must be used to infer physical variables (see below). The SFMR is used to estimate the 10 m wind speed from the upwelling microwave radiance. The wind speed algorithm is effective in the 15–75 m s^{-1} range [*Uhlhorn et al.,* 2007]. A total of 16 dropsondes were deployed on 5 October; these were used to check wind profiles but were not actually used in the processing except to compute radar attenuation by water vapor absorption.

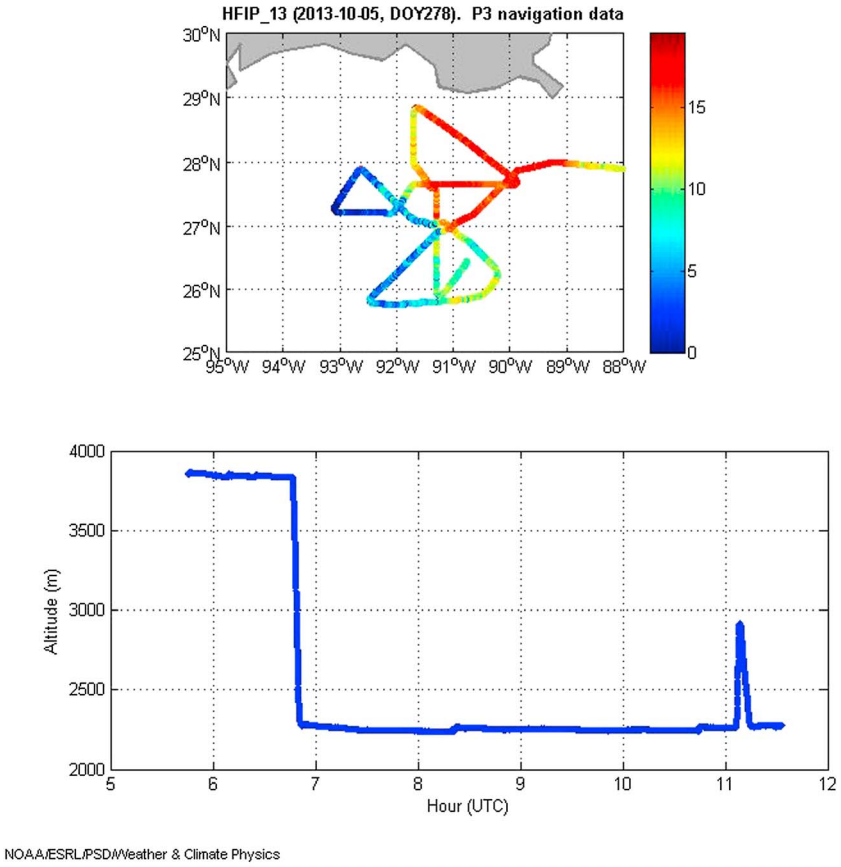

Figure 1. (Upper panel) Flight track for NOAA WP-3 aircraft on 5 October 2013. The color represents the wind speed from the Stepped Frequency Microwave Radiometer; colorbar indicates values of U_{10} (m s^{-1}). New Orleans is in the top of the map. The aircraft altitude during the sampling period is shown in the lower panel.

3. Data Processing

For this study we have used the Doppler moment files only (i.e., we have not reprocessed or re-analyzed the raw spectral files). From the radar calibration, the zeroth moment is related to the radar reflectivity factor, Z (usually expressed in log-form as reflectivity factor, dBZ). The radar total system (including the antenna) is calibrated to about ±1 dB [*Moran et al.*, 2012]. We have applied a correction to Z for the dielectric window the radar transmits through (1.6 dB) and an attenuation correction (about 4.0 dB) based on the column-integrated water vapor concentration from the aircraft to the range gate [*Li et al.*, 2005]. Attenuation by rain is well characterized and is not an issue because we are using nearly rain-free profiles. Uncertainty in these adjustments suggests that dBZ values are no better than ±2 dB, which is consistent with calculations of the radar cross section [*Li et al.*, 2005] for the ocean surface at W-Band obtained in light winds from a test flight (not shown).

The first moment of the Doppler spectrum (see section 4) is the Doppler shift in the radar beam radial direction. This shift is caused by motion of the scattering entities (clouds, rain, sea spray, insects, etc.) relative to the aircraft. Note, small drops essentially follow the air motions, but drops larger than a few 10's of micrometer radius have a mean (gravitational) slip velocity, V_g, relative to the air. Because of its short wavelength, the radar is essentially insensitive to Bragg (clear air) returns associated with atmospheric refractive index fluctuations [*White et al.*, 1996]. The second moment is related to the width of the droplet size spectrum [*Frisch et al.*, 1995] but with contaminating factors associated with turbulence and shear. We have estimated the broadening effects using *Shupe et al.* [2008] and found them negligible compared to the measured Doppler widths. The finite angular width of the radar beam (0.7°) convolved with the relative horizontal speed of the of the droplets (principally the speed of the aircraft) causes a Doppler

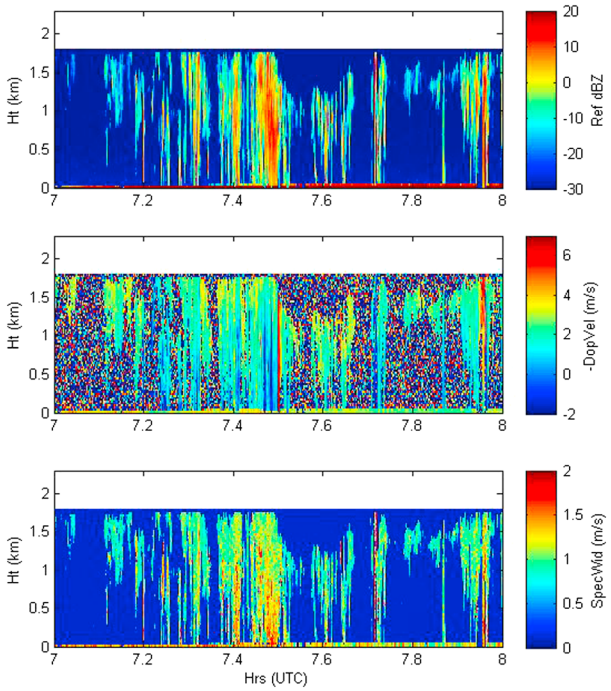

Figure 2. Time-height cross section of 1 h of Doppler moment data at 0.3 s time resolution from the ESRL radar on 5 October 2013: upper panel, radar reflectivity factor (dBZ); middle panel, raw Doppler radial velocity, $-V_r$; bottom panel, Doppler width. Height is measured positive upward with 0 being the surface; the white area between $z = 1.8$ and $z = 2.3$ km is because the first radar range gate is 500 m below the aircraft. The surface is seen as the bright horizontal line at height = 0 (the aircraft is at 2.3 km altitude). Bright red vertical bands on the upper panel denote precipitation; reflectivity less than −18 dBZ are principally clouds

broadening of about 0.45 m s^{-1} [*Heymsfield et al.*, 1996]. A complicating factor occurs because the retrieved values of Doppler width are increasingly underestimated as signal-to-noise ratio (SNR) approaches the detection threshold. We have computed a simple correction as a function of SNR obtained through Monte Carlo simulations of a Gaussian signal added to white noise.

We are analyzing for sea spray, so our emphasis is on signals obtained near the sea surface.

1. For each profile, we identify the surface return as the maximum Z in a range window computed from the aircraft altitude and pitch/roll. The vertical ordinate (height above the surface) is indexed from that point. The surface return contaminates the first one or two range gates above the maximum, so we consider the first usable data to be from a height of 75 m above the surface.
2. To eliminate contamination by rain, we exclude profiles where any range gate in the height range 500–1000 m has dBZ > -18. The threshold for light drizzle is normally −15 dBZ.
3. We are interested in obtaining values for V_g (a key microphysical parameter), but aircraft pitch and roll cause the measured radial Doppler velocity to be contaminated by the horizontal wind and the aircraft air speed. To correct for this, we use a standard rotational matrix method to relate the velocity components in the tilted frame to those in the earth frame [*Edson et al.*, 1998]. The measured Doppler velocity, V_{Dop}, is given by

$$V_{Dop} = V_{radial} = \hat{i}_r \cdot \left[G - U_w - V_g \hat{i}_z\right] \quad (1)$$

where **G** is the ground speed of the aircraft, $\mathbf{U_w}$ is the wind vector at the appropriate range gate, $\hat{i}_r$ is the unit vector in the radar beam (radial) direction, and $\hat{i}_z$ is the unit vector in the vertical direction. For this paper we have neglected the vertical components of G and U_w. Quantities in (1) are expressed in earth coordinates.

The radar radial is downward pointing in the aircraft frame. In the earth frame, it is given by

$$\hat{i}_r = \mathbf{T}(\theta, \phi, \psi) \cdot (0, 0, -1) \quad (2)$$

Here **T** is a matrix that rotates the radar radial to the earth frame [*Edson et al.*, 1998]. The aircraft orientation is specified by its pitch (θ), roll (ϕ), and heading (ψ). After multiplying the terms, we can solve for V_g

$$V_g = \left[V_N + V_E - V_{Dop}\right] / \left[\cos(\theta)\cos(\phi)\right] \quad (3)$$

Here V_N and V_E are the N and E components of $G - U_w$ dotted into $\hat{i}_r$; we assume that the mean vertical components of **G** and $\mathbf{U_w}$ are negligible. Because the dropsondes show weak shear in the 75–300 m region, we have used U_{10} from the SFMR to estimate U_w. The navigation information is unbiased to a few tenths of a

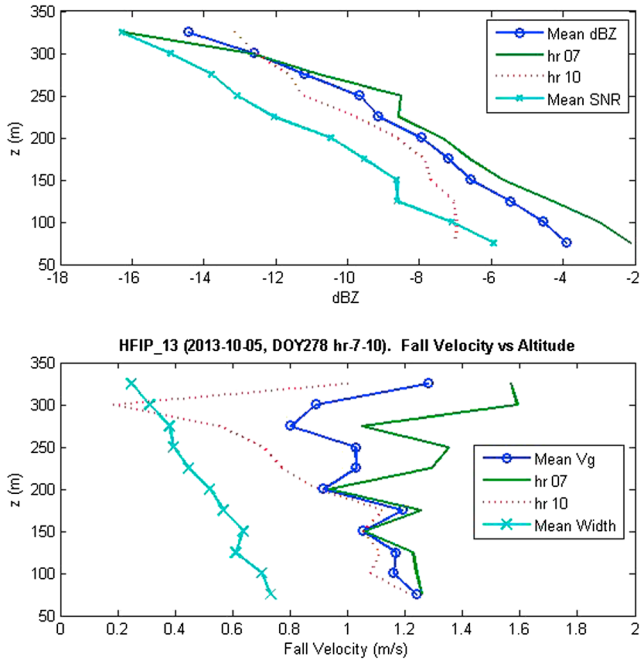

Figure 3. Mean profiles of radar moments from all valid data on 5 October 2013: SNR > -12 dB at z = 75 m, no rain in the column, and $U_{10} > 15$ m s^{-1}. Upper panel shows profiles of mean SNR and the mean reflectivity. Lower panel shows profiles of mean observed Doppler width (*x*'s) and mean droplet fall velocity deduced from mean Doppler velocity via equation (3).

degree and about 0.5 m s^{-1}. We have propagated these uncertainties through the equations to evaluate the sensitivity of the fall velocity retrieval. Only the pitch angle (which is directly convolved with the aircraft ground speed) contributes significantly to the uncertainty in V_g. To reduce this uncertainty, we determined the relative misalignment of the radar and the navigation system pitch measurement by comparing the measured Doppler velocity as a function of pitch for cloud returns (dBZ < -25, negligible fall velocity) in the range gates closest to the aircraft. We determined that the radar has a 1.1° tilt relative to the pitch sensor; a correction was applied for this analysis

4. Microphysical Analysis

The Doppler spectral moments have been processed to estimate sea-spray properties. To isolate the sea-spray signal, we eliminate contamination by rain by requiring that the reflectivity between 500 and 1000 m altitude does not exceed −18 dBZ. Weak rain is allowed above 1000 m altitude, provided that it does not attenuate the return from the surface. We assume that sea spray occurs in the high wind speed region, so we require $U_{10} > 15$ m s^{-1}. The wind speed threshold limits the data to hours 7, 9, and 10 UT. In these three hours, 24% of the profiles pass the rain-free, high wind speed requirement (call these RFHW). We have computed averages for the moments when sea spray is present in concentrations sufficient to yield good moment estimates. Thus, we identify all RFHW profiles with a signal-to-noise ratio (SNR) > -12 dB at $z = 75$ m. This SNR threshold assures good estimates of Doppler velocity. Only 2.3% of the RFHW profiles passed this criterion; if we look instead at $U_{10} < 15$ m s^{-1}, then no sea-spray return is obtained. The low fraction of sea-spray observations confirms the anticipated intermittent nature of spume drop production and the concept that there is a wind speed threshold for significant production. At these winds speed, we expect less than 1% areal coverage of actively breaking waves [*Hanson and Phillips*, 1999].

To assure a linear average of reflectivity, we convert the dBZ to *Z*, average, and then convert back. The average moments and SNR for the profiles containing surface-based returns (e.g., sea spray) are shown in Figure 3. Note, we have converted the first moment to V_g via (3) before averaging. We have shown mean profiles for each hour and the total average.

The next stage of analysis is based on the Gaussian moment-retrieval method of *Frisch et al.* [1995]. It is assumed that the drop size distribution, *n(r)*, can be represented by a log-normal distribution, which has three parameters: the mode drop radius, r_0; the total drop concentration, *N*; and the logarithmic width, σ_x. The *k*-th moment of this distribution is

$$< r^k >= r_0^k \exp\left(k^2 \sigma_x^2/2\right) \tag{4}$$

The radar backscatter cross section per unit volume, η, is related to the droplet concentration via the standard Rayleigh approximation

$$\frac{\partial \eta}{\partial r} = 4\pi(2\pi/\lambda)^4 |K|^2 r^6 n(r) \tag{5}$$

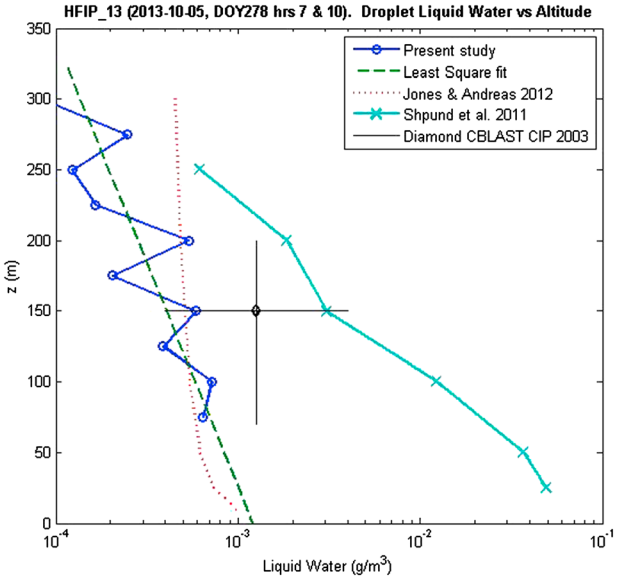

Figure 4. Sea-spray liquid water concentration (LWC) profile corresponding to data in Figure 3 (data are the circles and a least squares fit is the dashed line). The dotted line shows the parameterization of *Jones and Andreas* [2012] for $U_{10} = 18\ \mathrm{m\,s^{-1}}$. The *x*'s are from the numerical model study of *Shpund et al.* [2011] for $U_{10} = 25\ \mathrm{m\,s^{-1}}$. The diamond is the mean results from the Cloud Imaging Probe (CIP) from ten rain-free level runs ($<U_{10}> = 23\ \mathrm{m\,s^{-1}}$) on the NOAA WP-3 during Hurricanes Fabian and Isabel. The thin lines through the diamond denote the range of heights and LWC values.

Here λ is the radar wavelength, and $|K|^2 = 0.93$ is the refractive index factor of liquid water at the radar wavelength. Thus, η is the integral of (5) over all droplets:

$$\eta = \int \frac{\partial \eta}{\partial r} dr = \pi^5 \lambda^{-4} |K|^2 Z \tag{6}$$

Z is the reflectivity factor usually expressed in $\mathrm{dBZ} = 10 \times \mathrm{LOG}_{10}(Z) + 180$. Thus, the reflectivity (sixth moment of the size distribution) and liquid water content, q_l (third moment), are easily related. For drops in the 40–400 μm radius range, V_g is approximately linear in radius

$$r = aV_g + b \tag{7}$$

so the mean fall velocity of the distribution is the first moment of the droplet distribution. We used $a = 1.2 \times 10^{-4}$ s and $b = 1.0 \times 10^{-5}$ m.

The fundamental measurement of a Doppler radar is the Doppler spectrum, $\partial\eta/\partial V$, defined as the backscatter detected between Doppler velocities $V - dV/2$ and $V + dV/2$. Thus, the Doppler spectrum is related to the droplet spectrum (neglecting broadening effects) by

$$\frac{\partial \eta}{\partial V} = \frac{\partial \eta}{\partial r}\frac{\partial r}{\partial V_f} = 4\pi(2\pi/\lambda)^4 |K|^2 r^6 \frac{\partial r}{\partial V_f} n(r) \tag{8}$$

For the sea-spray radius region, the Doppler spectrum is linearly proportional to the size spectrum weighted by r^6. *Frisch et al.* [1995] show that Doppler spectral moments can be used to relate the Gaussian width, modal radius, and liquid water concentration.

$$\sigma_x = \left[\ln\left(1 + \sigma_v^2/\left(< V_g > + b/a\right)^2\right)\right]^{1/2} \tag{9a}$$

$$< Z > = \frac{48}{\pi}\left(a < V_g >\right)^3 (q_l/\rho_w) \exp\left(-6\sigma_x^2\right) \tag{9b}$$

$$a < V_g > + b = r_0 \exp\left(13\sigma_x^2/2\right) \tag{9c}$$

The measured parameters are the mean reflectivity ($<Z>$), the mean fall velocity ($<V_g>$), and the mean Doppler width (σ_V) shown in Figure 3. From these, we compute the logarithmic width (9a), the liquid water (9b), and the mode radius (9c). The observed Doppler width, after correction for its SNR dependence, is $0.82 \pm 0.04\ \mathrm{ms^{-1}}$ (independent of height). Correction for beam width broadening ($0.44\ \mathrm{ms^{-1}}$) gives $\sigma_v = 0.70\ \mathrm{ms^{-1}}$. In the samples with spray, there are approximately 100 drops $\mathrm{L^{-1}}$ with a mode radius of about 25 μm (mass-mode radius about 40 μm). These represent typical properties of the spray in those periods (2.3% of the time) *when it is present*; we assume zero liquid water in the other 97.7% of the samples. The true area-averaged liquid water content would be 2.3% of the retrieved value to account for the periods when no liquid is present. The profile of the final LWC area-averaged values is shown in Figure 4. The largest value shown here ($\sim 10^{-3}\ \mathrm{g\,m^{-3}}$) is about a factor of 100 less than a typical stratus cloud (10^5 drops $\mathrm{L^{-1}}$ of 10 μm radius).

5. Discussion

We can compare our results to other observations (admittedly limited) and examine the height dependence of concentration in the context of simple theory. The ±2 dB uncertainty in radar *Z* translates to a 60% uncertainty in our LWC retrievals. Uncertainty in V_g is more difficult to estimate. The V_N and V_E corrections are

about ±1 m s^{-1}, so their uncertainty is probably a small fraction of that. Note the variability between hourly retrievals at $z < 200$ m is fairly small—the uncertainty in mean retrieved V_g is on the order of ±0.2 m s^{-1}. The Gaussian droplet size distribution assumption requires three parameters, which is convenient given our basic three moments—but other three-moment distributions might be better. Given the uncertainties in Z and V_g, it is unlikely that more sophisticated statistics are justified. In summary, for good SNR values ($z < 200$ m), the uncertainty in retrieved LWC at a given height is no better than a factor of two. There is also some sensitivity of the values in the upper part of the profiles to the criteria used to select valid data.

The simplest scaling approach for drops produced at the surface follows from assuming a balance between the fall velocity (downward) and upward turbulent transport against a negative vertical concentration gradient [*Fairall et al.*, 1990; *Chamecki et al.*, 2007] so the net flux of drops is zero. In the surface layer, the turbulent eddy diffusion coefficient is given by $K = \kappa z u_*$ where $\kappa = 0.4$ is von Karman's constant and u_* is the friction velocity (estimated to be 0.8 m s^{-1} for our observations). At heights above the drop production region (say, z greater than wave height), the balance gives a simple differential equation

$$-K\partial n(r,z)/\partial z = V_g n(r,z) \tag{10}$$

The integration of (10) gives a relationship between the concentration at height z and another height h:

$$n(z) = n(h)(z/h)^{-\frac{V_g}{\kappa u_*}} \tag{11}$$

Because V_g is a strong function of radius, this implies steeper gradients as particle size increases. Using $V_g = 1.2$ m s^{-1}, $u_* = 0.8$ m s^{-1}, and $q_l = 8 \times 10^{-4}$ g m^{-3} at $z = 75$ m, equation (11) yields $q_l = 4 \times 10^{-5}$ g m^{-3} at $z = 300$ m. This is a somewhat steeper decrease with height than the dashed line in Figure 4.

Jones and Andreas [2012] have published a simple scaling model that combines a wind speed-dependent lognormal drop distribution at wave height and equation (11) that is tuned to their database of observations from the literature. *Shpund et al.* [2011] have used a surface source function from *Fairall et al.* [2009] in a 2-D large eddy turbulence model and given profiles of drop LWC for a specified $U_{10} = 25$ m s^{-1}. These estimates are shown in Figure 4 with the radar retrievals. The *Jones and Andreas* [2012] parameterization is based on 31 publications of in situ aerosol observations in the near-surface layer ($z = 0.1$–20 m) with wind speeds 0–29 m s^{-1}. Laboratory measurements provide a different perspective. At similar forcing, *Fairall et al.* [2009] found q_l values on the order of 2×10^{-2} gm^{-3}, but this was at 15 cm height above 10 cm waves in a wind tunnel. At stronger forcing, wind tunnel LWC values were nearly two orders of magnitude greater. Also shown in Figure 4 is a single point computed from the average droplet size spectrum of all usable observations from the CIP taken during the CBLAST flights near the surface in two hurricanes (nominal 10 m wind speed 23 m s^{-1}).

Our results are summarized in Figure 4 in which the retrievals of radar-derived LWC are comparable to several different estimates of varying applicability. The *Jones and Andreas* [2012] results are likely the most robust at heights on the order of 10 m, since they are based entirely on in situ observations of *n(r)* near the surface. The CBLAST results are made at ~100 m heights, but some uncertainty remains because of the difficulty of eliminating rain without information on the column above. Given the uncertainty in the radar retrievals, it is apparent that our data are within the envelope of other estimates—but a more definitive conclusion is elusive. The differences in the vertical gradient suggest that our radar observations imply somewhat larger drops than *Jones and Andreas* [2012] but smaller than *Shpund et al.* [2011]. Regardless, this paper demonstrates the potential of airborne Doppler millimeter-wavelength radar to greatly expand understanding of sea-spray production at high wind speeds. It is also important to note the limitations, particularly the inability of the current system to see drops close to the surface ($z < 75$ m). Clearly, more observations at true hurricane wind speeds are required.

Acknowledgments

The authors express appreciation to a legion of scientists, engineers, and staff at NOAA's AOC for their help and support in the amusing task of installing, testing, and flying a W-Band radar on the NOAA WP-3. Help of Terry Lynch, Dana Naeher, and Wayne Pullen is noted specifically. We acknowledge the cooperation and support of Jim McFadden, Frank Marks, and Paul Reasor for the entire project. We also thank David Richter and Jorgen Jensen for their thoughtful reviews. The data for this project are available at ftp://ftp1.esrl.noaa.gov/psd3/cruises/W-Band-P3/P3-20131005/.

The Editor thanks Jorgen Jensen and an anonymous reviewer for their assistance in evaluating this manuscript.

References

Andreas, E. L., J. B. Edson, E. C. Monahan, M. P. Rouault, and S. D. Smith (1995), The spray contribution to net evaporation from the sea – A review of recent progress, *Boundary Layer Meteorol.*, *72*, 3–52.

Andreas, E. L., and K. A. Emanuel (2001), Effects of sea spray on tropical cyclone intensity, *J. Atmos. Sci.*, *58*, 3741–3751.

Andreas, E. L. (2004), Spray stress revisited, *J. Phys. Oceanogr.*, *34*, 1429–1440.

Bao, J.-W., C. W. Fairall, S. A. Michelson, and L. Bianco (2011), Parameterizations of sea-spray impact on the air-sea momentum and heat fluxes, *Mon. Weather Rev.*, *139*, 3781–3797, doi:10.1175/MWR-D-11-00007.1.

Bianco, L., J.-W. Bao, C. W. Fairall, and S. A. Michelson (2011), Impact of sea spray on the surface boundary layer, *Boundary Layer Meteorol.*, *140*, doi:10.1007/s10546-011-9617-1.

Black, P. G., E. A. D'Asaro, T. B. Sanford, W. M. Drennan, J. A. Zhang, J. R. French, P. P. Niiler, E. J. Terrill, and E. J. Walsh (2007), Air-sea exchange in hurricanes: Synthesis of observations from the coupled boundary layer air-sea transfer experiment, *Bull. Am. Meteorol. Soc.*, *88*, 357–374, doi:10.1175/BAMS-88-3-357.

Chamecki, M., R. van Hout, C. Meneveau, and M. B. Parlange (2007), Concentration profiles of particles settling in the neutral and stratified atmospheric boundary layer, *Boundary Layer Meteorol.*, *125*, 25–38.

Drennan, W. M., J. A. Zhang, J. R. French, C. McMormick, and P. G. Black (2007), Turbulent fluxes in the hurricane boundary layer. Part II: Latent heat flux, *J. Atmos. Sci.*, *64*, 1103–1115.

Edson, J. B., A. A. Hinton, K. E. Prada, J. E. Hare, and C. W. Fairall (1998), Direct covariance flux estimates from moving platforms at sea, *J. Atmos. Oceanic Technol.*, *15*, 547–562.

Edson, J. B., J. V. S. Raju, R. A. Weller, S. Bigorre, A. Plueddemann, C. W. Fairall, S. Miller, L. Mahrt, D. Vickers, and H. Hersbach (2013), On the exchange of momentum over the open ocean, *J. Phys. Oceanogr.*, *43*, 1589–1610, doi:10.1175/JPO-D-12-0173.1.

Emanuel, K. A. (1995), Sensitivity of tropical cyclones to surface exchange coefficients and a revised steady-state model incorporating eye dynamics, *J. Atmos. Sci.*, *52*, 3969–3976.

Esteban-Fernandez, D., S. L. Durden, J. Chaubell, and K.B. Cooper (2010), Design considerations for a dual-frequency radar for sea spray measurement in hurricanes, *Geoscience and Remote Sensing Symposium (IGARSS), 2010 IEEE International*, 2896-2899, 25-30, doi:10.1109/IGARSS.2010.5653198.

Fairall, C. W., J. B. Edson, and M. A. Miller (1990), Heat fluxes, whitecaps, and sea spray, in *Surface Waves and Fluxes: Current Theory and Remote Sensing*, edited by G. Geernaert and W. Plant, pp. 173–208 , D. Reidel, Dordrecht, Netherlands.

Fairall, C. W., J. D. Kepert, and G. H. Holland (1994), The effect of sea spray on surface energy transports over the ocean, *Global Atmos. Ocean Syst.*, *2*, 121–142.

Fairall, C. W., E. F. Bradley, J. E. Hare, A. A. Grachev, and J. B. Edson (2003), Bulk parameterization of air-sea fluxes: Updates and verification for the COARE algorithm, *J. Clim.*, *16*, 571–591.

Fairall, C. W., M. Banner, W. Peirson, R. P. Morison, and W. Asher (2009), Investigation of the physical scaling of sea spray spume droplet production, *J. Geophys. Res.*, *114*, C10001, doi:10.1029/2008JC004918.

Frisch, A. S., C. W. Fairall, and J. B. Snider (1995), Measurement of stratus cloud and drizzle parameters in ASTEX with a K_α -band Doppler radar and a microwave radiometer, *J. Atmos. Sci.*, *52*, 2788–2799.

Hanson, J. L., and O. M. Phillips (1999), Wind sea growth and dissipation in the open ocean, *J. Phys. Oceanogr.*, *29*, 1633–1648.

Heymsfield, G. M., S. W. Bidwell, I. J. Caylor, S. Ameen, S. Nicholson, W. Boncyk, L. Miller, D. Vandemark, P. E. Racetter, and L. R. Dod (1996), The EDOP radar system on the high-altitude NASA ER-2 aircraft, *J. Atmos. Oceanic Technol.*, *13*, 795–809.

Jones, K. F., and E. L. Andreas (2012), Sea spray concentrations and the icing of fixed offshore structures, *Q. J. R. Meteorol. Soc.*, *138*, 131–144.

Kepert, J. D., C. W. Fairall, and J.-W. Bao (1999), Modeling the interaction between the atmospheric boundary layer and evaporating sea spray droplets, in *Air-Sea Fluxes: Momentum, Heat, and Mass Exchange*, edited by G. L. Geernaert, pp. 363–409 , Kluwer, Dordrecht, Netherlands.

Kudryavtsev, V. N., and V. K. Makin (2011), Impact of ocean spray on the dynamics of the marine atmospheric boundary layer, *Boundary Layer Meteorol.*, *140*, 383–410, doi:10.1007/s10546-011-9624-2.

Li, L., G. M. Heymsfield, L. Tian, and P. E. Racette (2005), Measurements of ocean surface backscattering using an airborne 94-GHz cloud radar – implications for calibration of airborne and spaceborne W-Band radars, *J. Atmos. Oceanic Technol.*, *22*, 1033–1045.

Moran, K., S. Pezoa, C. W. Fairall, C. Williams, T. Ayers, A. Brewer, S. P. de Szoeke, and V. Ghate (2012), A motion-stabilized W-band radar for shipboard observations of marine boundary-layer clouds, *Boundary Layer Meteorol.*, *141*, 3–24, doi:10.1007/s10546-011-9674-5.

Richter, D., and P. Sullivan (2014), The sea spray contribution to sensible heat flux, *J. Atmos. Sci.*, *71*, 640–654, doi:10.1175/JAS-D-13-0204.1.

Shpund, J., J. A. Zhang, M. Pinsky, and A. Khain (2011), Microphysical structure of the marine boundary layer under strong wind and spray formation as seen from simulations using a 2D explicit microphysical model. Part I: The impact of large eddies, *J. Atmos. Sci.*, *68*, 2366–2384, doi:10.1175/2011JAS3652.1.

Shupe, M. D., K. Pavlos, M. Poellot, and E. Eloranta (2008), On deriving vertical air motions from cloud radar Doppler spectra, *J. Atmos. Oceanic Technol.*, *25*, 547–557, doi:10.1175/2007JTECHA1007.1.

Toffoli, A., A. V. Babanin, M. A. Donelan, B. K. Haus, and D. Joeng (2011), Estimating sea spray volume with a laser altimeter, *J. Atmos. Oceanic Technol.*, *28*, 1177–1183.

Uhlhorn, E. W., P. G. Black, J. L. Franklin, M. Goodberlet, J. Carswell, and A. S. Goldstein (2007), Hurricane surface wind Measurements from an operational stepped frequency microwave radiometer, *Mon. Weather Rev.*, *135*, 3070–3085, doi:10.1175/MWR3454.1.

Walsh, E. J., D. W. Hancock, D. E. Hines, R. N. Swift, and J. F. Scott (1985), Directional wave spectra measured with the surface contour radar, *J. Phys. Oceanogr.*, *15*, 566–592.

White, A. B., C. W. Fairall, A. S. Frisch, B. W. Orr, and J. B. Snider (1996), Recent radar measurements of turbulence and microphysical properties in clouds, *Atmos. Res.*, *40*, 177–121.

Yurovsky, Y. Y., and V. V. Malinovsky (2012), Radar backscattering from breaking wind waves: Field observation and modelling, *Int. J. Remote Sens.*, *33*(8), 2462–2481, doi:10.1080/01431161.2011.614966.